ELSEVIER

Journal of Nuclear Materials 253 (1998) 120–132

journal of nuclear materials

Microstructure of Al_2O_3 and $MgAl_2O_4$ irradiated at low temperatures

S.J. Zinkle [a,*], G.P. Pells [b]

[a] *Metals and Ceramics Division, Oak Ridge National Laboratory, Oak Ridge, TN 37831-6376, USA*
[b] *Materials and Chemistry Group, AEA Technology, Harwell Laboratory, Oxon OX11 0RA, UK*

Abstract

Polycrystalline specimens of aluminum oxide (99.9% purity) and stoichiometric magnesium aluminate spinel ($MgAl_2O_4$) were irradiated with 4 MeV Ar^+ ions at 200 and 300 K to doses of 0.1 to 10 displacements per atom (dpa). Volumetric swelling was determined from step-height and lattice parameter measurements. The step-height swelling increased with decreasing irradiation temperature, with values of $\sim$4.5% and $\sim$0.8% in Al_2O_3 and $MgAl_2O_4$, after $\sim$10 and 5 dpa at 200 K, respectively. Faulted interstitial dislocation loops lying on {111} planes were observed in spinel irradiated at 200 and 300 K, indicating the presence of significant interstitial mobility at both temperatures. Dislocation loops and network dislocations were observed in alumina following irradiation at 300 K, but resolvable defect clusters did not form at 200 K. Amorphization was not observed in any of the specimens. The critical temperature for amorphization is predicted to be slightly below 200 K for alumina irradiated at $\sim 10^{-4}$ dpa/s. Due to the higher defect mobility in spinel compared to alumina, the critical temperature for amorphization in spinel is expected to be significantly lower than that of alumina.

1. Introduction

Numerous studies have been performed on the microstructural changes of Al_2O_3 and $MgAl_2O_4$ (spinel) following energetic particle irradiation at temperatures above room temperature [1–21]. These studies were motivated by interest in fundamental aspects of displacement damage in model ceramic insulators with predominantly ionic bonding, and also by the desire to identify radiation-resistant ceramics for heating, diagnostics, and insulator applications for fission and fusion energy devices. The key trends identified in these elevated temperature studies are that the swelling levels in irradiated alumina are considerably higher than that of spinel (e.g., $\sim$3% volumetric swelling in alumina vs. $\sim$0% swelling in spinel after fission neutron irradiation to 10 displacements per atom at 923 K), and that the concentration of dislocation loops and network dislocations is generally much higher in alumina compared to spinel [4,18,22]. Several different mechanisms have been proposed to explain this difference in irradiated behavior, including the higher number of interstitials needed to form a stoichiometric loop nucleus in spinel compared to alumina (seven vs. five interstitials) [18,23], the relatively high difficulty of dislocation loop unfaulting in spinel (presumably associated with either a relatively low stacking fault energy or else the inability to nucleate an $a/4\langle 112\rangle$ partial dislocation) [4], efficient recombination of interstitials with structural vacancies in the spinel lattice (related to the relative ease of Mg and Al cation disordering in spinel) [18,21], and high amounts of ionization-induced point defect diffusion and/or recombination in spinel [14–16]. It has also been recently noted that the rate-controlling interstitial migration energy for loop formation in spinel is considerably smaller than in Al_2O_3 (0.21 vs. $\sim$0.6 eV), which would produce a significantly lower interstitial loop nucleation rate in spinel [24].

In recent years there has been increasing interest in the microstructural evolution of ceramic insulators irradiated at or below room temperature. This has been driven in part by fusion reactor designs which require most insulators to be water cooled, and the insulators for electron cyclotron and neutral beam injection heating systems may have to be cooled to cryogenic temperatures. In addition, many of these low-temperature studies were sparked by the desire

* Corresponding author. Tel.: +1-423 576 7220; fax: +1-423 574 0641; e-mail: zinklesj@ornl.gov.

0022-3115/98/$19.00
PII S0022-3115(97)00323-1

to understand the conditions which lead to amorphization in irradiated materials. The results from several studies indicate Al_2O_3 can be completely amorphized following heavy ion irradiation to a dose of ~3 to 6 displacements per atom (dpa) at temperatures below 80 K [25–28], where the damage levels were calculated assuming a sublattice-averaged displacement energy of 40 eV. The threshold dose to produce complete amorphization in alumina increases at higher temperatures, although the specific values are dependent on damage rate and also appear to be dependent on irradiation spectrum [27,28]. For example, Wang et al. [28] reported that the threshold amorphization dose for alumina irradiated with 1.5 MeV Xe ions at 10^{-3} dpa/s increased from ~5 dpa to ~10 dpa as the irradiation temperature was raised from 20 K to 83 K. On the other hand, Abe et al. [27] found that the threshold dose for amorphization of alumina irradiated with either 600 keV Kr or 900 keV Xe ions at 0.01–0.2 dpa/s was constant (~4 dpa) for irradiation temperatures between 90 K and 160 K, with a second plateau dose for complete amorphization of ~7 dpa observed at irradiation temperatures between 160 K and 200 K. The threshold dose for amorphization of alumina at temperatures above 200 K increased rapidly and was a strong function of irradiating species and particle flux [27]. Amorphization of Al_2O_3 at room temperature only occurs for certain ion species and generally does not occur until the dose is extremely high (>100 dpa), with concomitant implanted ion levels on the order of 50 at.% [25,29]. This suggests that the room temperature amorphization behavior of Al_2O_3 is dependent on the implantation of certain chemical species, rather than a simple displacement damage effect [25].

The amorphization behavior of spinel is not as well-known as that of alumina, although it appears to be resistant to amorphization. Amorphization was not observed in spinel irradiated with 1.5 MeV Kr ions at 20 K up to a maximum dose of 11 dpa [30,31], whereas partial amorphization occurred if the foil was pre-implanted with Ne ions [30]. Similarly, amorphization was not observed in spinel irradiated with 12 MeV Au ions to a maximum dose of 33 dpa at a nominal temperature of 100 K, although the authors speculated that beam heating may have raised the specimen temperature above 100 K [32]. Amorphization of spinel has been reported to occur at a threshold dose of ~35 dpa in spinel irradiated with 1.5 MeV Xe ions at 30 K [33]. Several other studies have observed somewhat lower threshold doses for amorphization of 12 to 25 dpa following 370–400 keV Xe ion irradiation at 100 to 170 K [32,34–36]. The implanted Xe concentrations in these studies were ~2 at.%. A recent study [37] suggested that $MgAl_2O_4$ could be amorphized at room temperature with 60 keV Xe ions at a dose rate of ~0.1 dpa/s after a dose of ~27 dpa (~3 at.% implanted Xe), although this disagrees with other room temperature studies which did not observe room temperature amorphization at somewhat lower damage rates of ~0.005 dpa/s up to 70 dpa [29]. In summary, it appears that spinel is more resistant to amorphization than Al_2O_3 for irradiation temperatures down to ~20 K, although further work is needed to quantify the detailed dose and temperature dependence of amorphization.

The purpose of the present study is to summarize macroscopic swelling (obtained from step height measurements) and microstructural observations on polycrystalline Al_2O_3 and $MgAl_2O_4$ specimens irradiated with 4 MeV Ar ions at 200 and 300 K. A brief description of the swelling measurements for the Al_2O_3 specimens has been previously published [38].

2. Experimental procedure

The polycrystalline materials for this study were a commercial grade of 99.9% Al_2O_3 (Vitox, Morgan Matroc, ~1.5 μm grain size) and 99.9% $MgAl_2O_4$ (0.6 μm sintered grain size) which was produced by isostatic pressing and air sintering of powder supplied by Baikowski International. The $10 \times 10 \times 1$ mm specimens were polished to a surface roughness of <20 nm and then irradiated with 4 MeV Ar^+ ions using the Harwell Van de Graaff accelerator. A tantalum mask was used to produce a well-defined 3×3 mm irradiated region on the specimens. The samples were rocked at an angle between 0 and 70° with respect to the sample normal with a cycle time of ~7 s in order to obtain a uniform damage profile at depths between ~0.4 and 1.7 μm. The sample holder was cooled via a flexible copper strap attached to a cold finger containing flowing nitrogen gas cooled to ~100 K. The specimen temperature was monitored by a chromel–alumel thermocouple which was in firm contact with the back (nonirradiated) face of the edge-cooled specimen. Beam heating considerations limited the lowest controllable irradiation temperature to 200 K. Typical beam currents during the irradiation were 0.1 $\mu A/cm^2$ at 200 K and 0.5 $\mu A/cm^2$ at 300 K. According to beam heating measurements on ceramic specimens in this target holder, the temperature difference between the irradiated surface and the thermocouple was <3°C for beam currents up to 0.5 $\mu A/cm^2$. The damage dose was calculated with the TRIM code [39], using threshold displacement energies in Al_2O_3 of 20 eV and 50 eV [40] for the aluminum and oxygen sublattices, respectively. Damage calculations were not performed for $MgAl_2O_4$ due to uncertainties in the sublattice displacement energies [40], although damage values similar to Al_2O_3 are expected based on kinematic considerations. Specimens were irradiated to ion fluences between 1×10^{19} and 1×10^{21} Ar^+/m^2 (~0.1–10 dpa). Further experimental details are given elsewhere [38,41–43].

Following irradiation, the step-height swelling was measured using a Sloan Dektak II surface profilometer. The typical resolution limit at the transition between the

masked and irradiated areas was ~5 nm, which corresponds to a volumetric swelling level of ~0.3%. The volumetric swelling was estimated from the step height swelling by invoking the standard assumption that all of the swelling in the ~1.5 μm × 3 mm × 3 mm irradiated region occurred normal to the surface, due to lack of constraint in this direction and the strong lateral constraint associated with the underlying unirradiated material.

Four of the specimens were subsequently glued to unirradiated polished specimens, sectioned and thinned by mechanical grinding and ion beam milling for cross-sectional transmission electron microscope (TEM) observation, using standard [44] procedures. The irradiation conditions of the specimens selected for TEM analysis were 10 dpa for the alumina specimens and 5 dpa for the spinel specimens, with specimens prepared for both irradiation temperatures of 200 K and 300 K. The TEM analysis was performed in a Philips CM12 electron microscope operating at 120 keV. The defect microstructure was analyzed using a combination of conventional bright field and weak beam dark field imaging conditions. The point defect volumetric swelling was measured by obtaining low-index electron diffraction patterns in large grains which spanned both irradiated and unirradiated regions. A minimum of four different grains were investigated for each irradiation condition. Diffraction patterns were taken in the unirradiated and irradiated regions without changing the magnetic lens current settings, thereby allowing the nonirradiated regions in the cross section specimens to serve as a calibration standard for the irradiated lattice parameters. The volumetric lattice parameter swelling was calculated from the lattice parameter measurements using the following well-known standard formulas: $\Delta V/V = 3(\Delta a/a)$ for the cubic spinel structure, and $\Delta V/V = \Delta c/c + 2(\Delta a/a)$ for alumina, where the standard [7,45] hexagonal close packed description for the rhombohedral α-Al_2O_3 crystal structure was used. The lattice parameter measurements were resolved into components perpendicular and parallel to the irradiated surface (i.e., unconstrained and constrained directions) for the lattice swelling calculations. Only the unconstrained direction was used for the lattice parameter swelling calculation.

3. Results

Fig. 1 summarizes the step-height swelling measurements as a function of damage level for alumina and spinel. It can be seen that the swelling generally increased with increasing dose, with no indication of saturation up to the maximum dose investigated (~10 dpa). The swelling in spinel was much lower than that in alumina for comparable irradiation conditions. The temperature dependence of the swelling was rather weak for both materials in this temperature range. The measured swelling in spinel irradiated at 200 K was similar to that observed at 300 K at all doses. The step-height swelling in alumina irradiated at 200 K appeared to be slightly higher than at 300 K, although the experimental uncertainties of the swelling for the two temperatures overlapped.

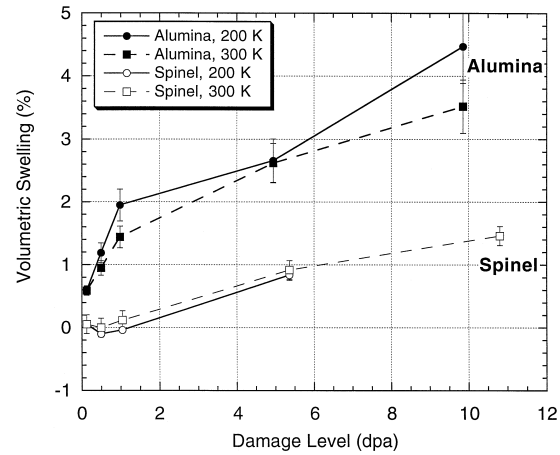

Fig. 1. Volumetric swelling of spinel and Vitox alumina as a function of 4 MeV Ar ion dose for irradiation temperatures of 200 and 300 K, as determined from step-height measurements.

3.1. Microstructure of irradiated Al_2O_3

The general microstructure of alumina irradiated to 10 dpa at 200 K and 300 K is shown in Fig. 2. A dramatic difference in the microstructure of these two specimens is evident from this figure. Whereas a high density of dislocation loops and network dislocations were present in the specimen irradiated at 300 K, resolvable loops were not observed in the alumina specimen irradiated at 200 K. Cavity formation was not visible at either irradiation temperature using standard through-focus kinematical imaging conditions (resolution limit ~2 nm diameter).

The defect microstructure of alumina irradiated to 10 dpa at 300 K is shown in more detail in Fig. 3. A mixture of dislocation loops and network dislocations were observed in the irradiated region. The average diameter of the loops was ~8 nm on both the basal (0001) and prism $\{1\bar{1}00\}$ habit planes. The loop density was $\sim 2 \times 10^{22}/\mathrm{m}^3$, with the majority of loops lying on the prism habit planes. According to previous studies on alumina irradiated with electrons, ions or neutrons at temperatures >770 K, stoichiometric edge-type interstitial loops are initially nucleated on the basal and prism habit planes with Burgers vectors of $\frac{1}{3}[0001]$ and $\frac{1}{3}\langle 1\bar{1}00\rangle$, respectively [2–5]. With continued irradiation, these loops nucleate a shear partial dislocation and eliminate the cation stacking fault, resulting in Burgers vectors of the type $\frac{1}{3}\langle 10\bar{1}1\rangle$ on both the basal and prism habit planes. This unfaulting occurred for loops larger than 15 to 100 nm diameter [2,5]. At high doses, the loops intersected to form a dislocation network

Fig. 2. General microstructure of alumina irradiated to 10 dpa at 200 K and 300 K.

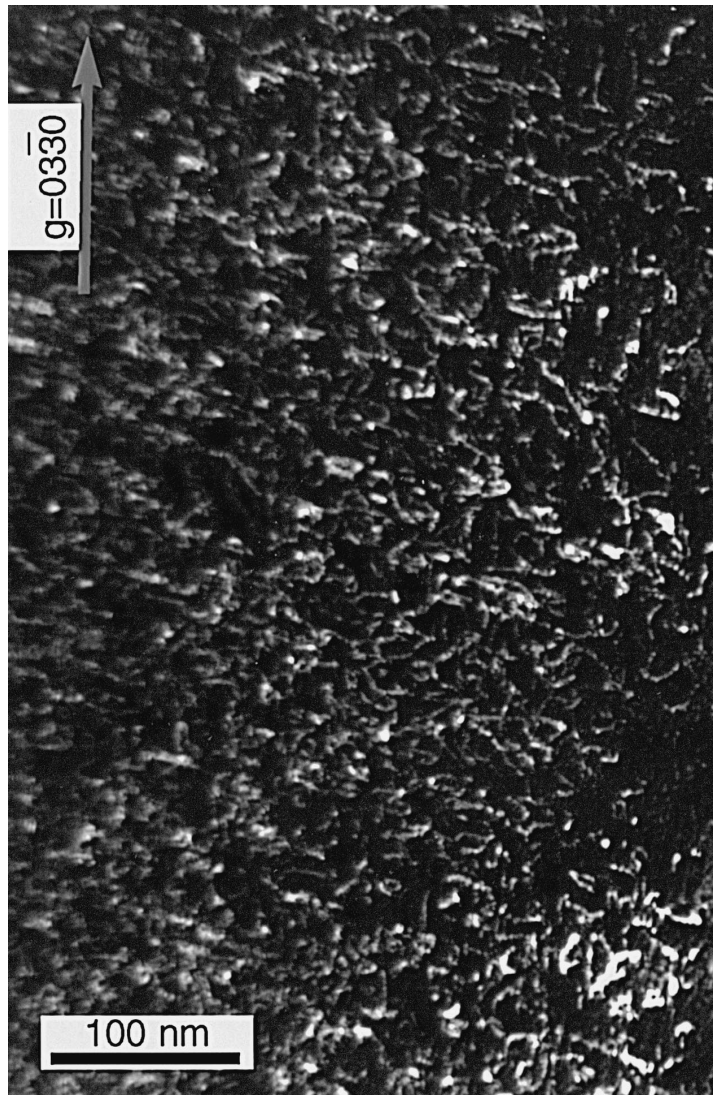

Fig. 3. Weak beam dark field micrograph of alumina irradiated to 10 dpa at 300 K. The image was taken near the $[2\bar{1}\bar{1}0]$ zone axis using $(g, 3g)$, $g = 03\bar{3}0$ diffraction conditions.

with predominant Burgers vectors of $\frac{1}{3}\langle 10\bar{1}1\rangle$ and $\frac{1}{3}\langle 1\bar{2}10\rangle$.

Although a detailed loop analysis was not performed, the defects in the alumina specimen irradiated to 10 dpa at 300 K exhibited contrast that suggested a variety of Burgers vectors were present. Streaking along 0006 directions was observed in the electron diffraction patterns, indicating the presence of faulted dislocation loops on the basal plane. However, some loops on the basal plane were also visible with $g = 11\bar{2}0$ or $03\bar{3}0$ diffraction vectors, indicating that a portion of the loops on the basal plane had a prism component to their Burgers vector. Similarly, some of the loops on the $\{1\bar{1}00\}$ habit planes could be imaged using $g = 0006$, implying that these loops had a basal component to their Burgers vector. The presence of a significant network dislocation density in the alumina specimen irradiated to 10 dpa at 300 K (Fig. 3) suggests that a significant amount of loop unfaulting and interaction has occurred.

3.2. Microstructure of irradiated $MgAl_2O_4$

As shown in Figs. 4 and 5, the microstructure of spinel irradiated to 5 dpa at both 200 K and 300 K consisted of a high density of small defect clusters. Cavity formation (2 nm resolution limit) was not observed in either of the specimens. Network dislocations were also not observed. The defect clusters in the irradiated spinel specimens were

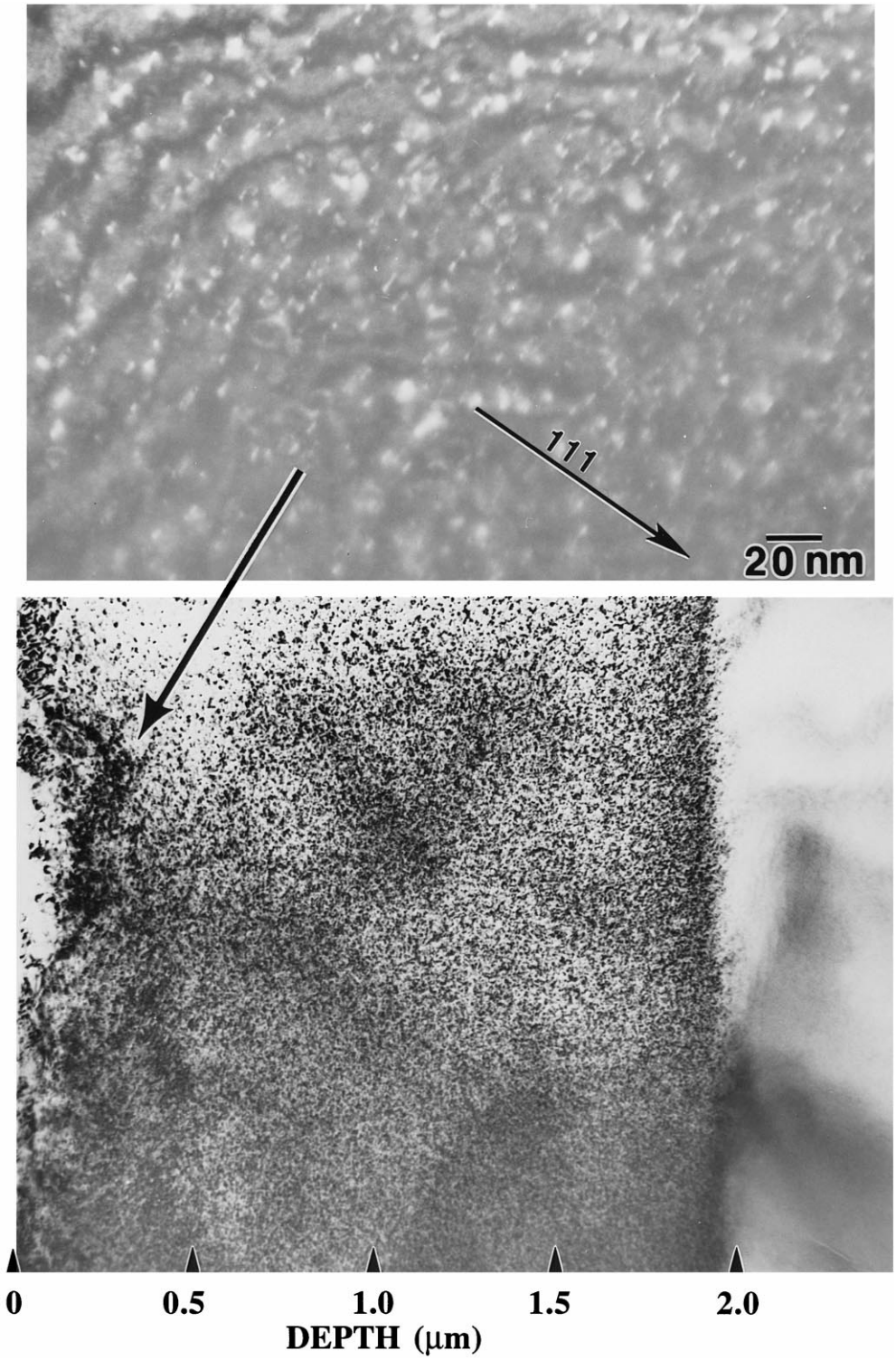

Fig. 4. Microstructure of spinel irradiated to 5 dpa at 200 K. The weak beam dark field image was obtained near the [110] zone axis using $(g, 3g)$, $g = 004$ diffraction conditions.

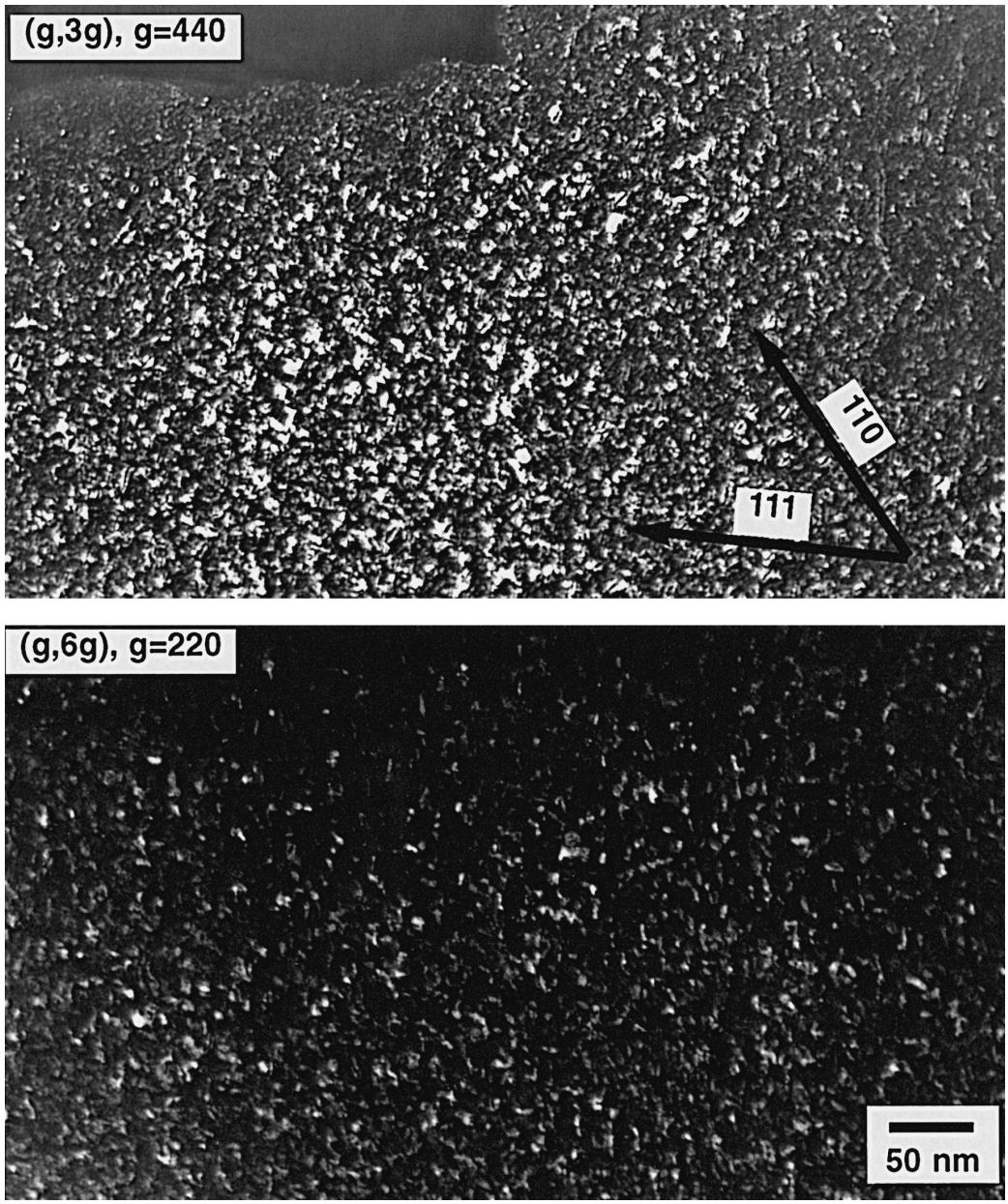

Fig. 5. Weak beam dark field (g, $3g$ and g, $6g$) micrographs obtained near the [$1\bar{1}0$] zone axis showing dislocation loops in spinel irradiated to 5 dpa at 300 K.

predominantly located on {111} habit planes. A small fraction (< 10% of total population) of the defect clusters were located on {110} and intermediate planes, which are presumably dislocation loops rotating on their glide cylinder from {111} to {110}. An example of loops on intermediate habit planes is shown in Fig. 6 for spinel irradiated at 200 K. There was no significant difference in the loop size or density for the two irradiation temperatures. The measured loop diameter and density were 4.4 nm and 5×10^{23} m^{-3} in the spinel specimen irradiated at 200 K, and 4.6 nm and 4×10^{23} m^{-3} in the spinel specimen irradiated at 300 K. Stacking fault fringes were generally not visible in the loop interiors for typical weak beam imaging conditions using $g = 002$ or 220. However, considering the effective extinction distance for the (g, $3g$) to (g, $6g$) weak beam imaging conditions used in this study, the expected fringe spacing in spinel for inclined faulted loops (Burgers vector $a/6\langle 111\rangle$) would be comparable to the

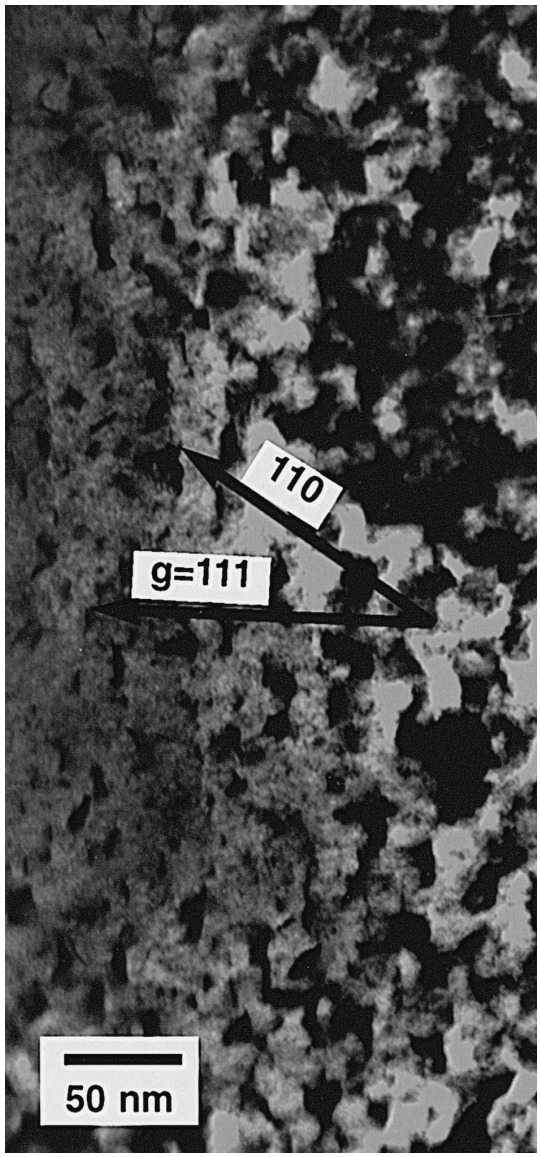

Fig. 6. Centered dark field micrograph obtained near the $[1\bar{1}0]$ zone axis showing defects on several habit planes in spinel irradiated to 5 dpa at 200 K.

4.5 nm loop diameter. Therefore, the fringes in faulted loops would not be visible due to the small loop size. Fault fringes were observed in some of the larger loops for $g = 440$ weak beam conditions, where the effective extinction distance (~ 2.4 nm for $(g, 4g)$ conditions) is sufficiently small to allow the fringes to be visible for inclined loops with diameters above ~ 4 nm. The interstitial vs. vacancy nature of the loops was not determined due to their small size. Previous studies on spinel irradiated at room temperature and high temperatures have only observed interstitial-type dislocation loops [10,12,17–20,23,46], and it would appear unlikely that the vacancy migration necessary for vacancy loop nucleation could occur in spinel irradiated near or below room temperature.

A high density of defects in the spinel specimens irradiated at both 200 K and 300 K could be imaged in centered or weak beam dark field using $g = \langle 222 \rangle$ diffraction vectors, which is a weakly diffracting condition for the spinel structure due to its near-zero electron structure factor (only the octahedral cations contribute to the 222 spot intensity). Fig. 7 shows an example of defects which were imaged in spinel irradiated to 5 dpa at 200 K using $(g, 4g)$, $g = 222$ conditions. Defects on the $(11\bar{1})$ habit plane were visible using a diffraction vector of $g = 222$, whereas defects on the (111) habit plane were selectively imaged using $g = 22\bar{2}$. The diffraction contrast analysis of these defects could be consistently attributed to an $a/6\langle 111 \rangle$ type stacking fault, indicating that the defects were $a/6\langle 111 \rangle\{111\}$ faulted (Frank) loops. Edge-on $a/4\langle 110 \rangle\{111\}$ dislocation loops would always have weak contrast ($g \cdot b = 0$ or an integer) for this imaging condition.

A small fraction ($< 10\%$) of the loops in spinel irradiated at 200 K and 300 K were analyzed to have Burgers vectors of $b = a/4\langle 110 \rangle$, which is unfaulted on anion sublattice. Previous work has reported that the dislocation loops in spinel irradiated at or above room temperature evolve through a sequence of Burgers vectors and habit planes with increasing dose [12,17–19]. The key steps in the evolution sequence are $a/6\langle 111 \rangle\{111\}$ (Frank edge-type loop with cation and anion stacking faults), $a/4\langle 110 \rangle\{111\}$ (mixed edge/screw loop faulted on cation sublattice only), $a/4\langle 110 \rangle\{110\}$ (rotation along glide cylinder to form prismatic loop with cation fault), $a/2\langle 110 \rangle\{110\}$ (perfect loop), and finally growth and interaction of the loops to produce a dislocation network. It appears that the spinel specimens irradiated to 5 dpa at 200 K and 300 K in the present study are between the first and second steps of this loop evolution sequence.

Fig. 8 compares the [110] zone axis electron diffraction patterns for spinel irradiated at 200 K and 300 K. A slight weakening of the first order reflections relative to the (440) systematic reflections is visible for the specimen irradiated at 200 K. Previous work has reported pronounced weakening of first order reflections in spinel irradiated at low temperatures as evidence for a new metastable spinel phase that is a precursor to amorphization [34,36,47–49]. Transformation to this metastable phase did not occur for the irradiation conditions investigated in the present study. It has been suggested that the change in space group (crystal symmetry) for the metastable spinel phase may be a natural consequence of cation disordering due to irradiation [30,50,51].

3.3. Lattice parameter expansion in irradiated Al_2O_3 and $MgAl_2O_4$

Table 1 summarizes the volumetric swelling calculated from the electron diffraction pattern and step-height mea-

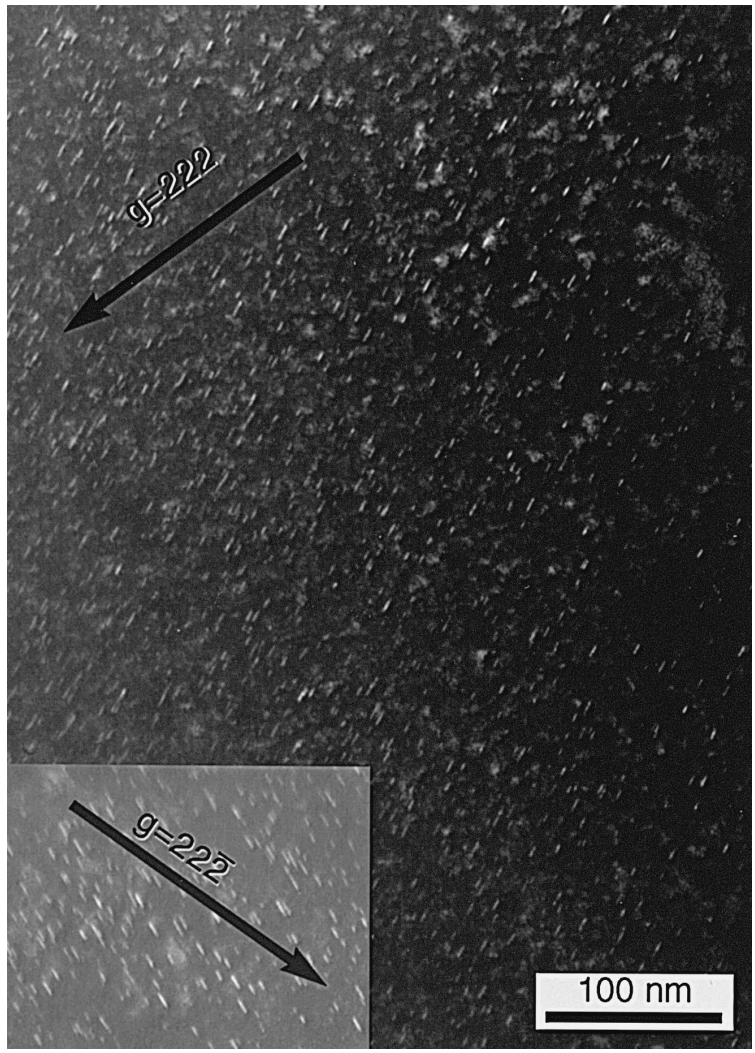

Fig. 7. Weak beam dark field $(g, 4g)$, $g = \langle 222 \rangle$ micrographs obtained near the $[1\bar{1}0]$ zone axis showing defects on the $(11\bar{1})$ and (111) habit planes in spinel irradiated to 5 dpa at 200 K.

surements for the four alumina and spinel specimens examined by TEM. No significant anisotropy in lattice parameter swelling was observed along the basal vs. prism planes in the irradiated alumina specimens. Good agreement was achieved between the step-height and lattice parameter expansion data for spinel irradiated at 200 and 300 K, with both measurements indicating relatively low levels of swelling of $< 1\%$ at both temperatures. On the other hand, the volumetric swelling calculated from electron diffraction patterns was significantly smaller than that measured in the step height measurements for both alumina specimens.

Previous studies on neutron-irradiated alumina at 350–900 K have found that the lattice parameter swelling matches the macroscopic swelling for doses up to ~ 0.5 dpa [1], but the lattice parameter swelling subsequently decreases and becomes much lower than the monotonically increasing macroscopic swelling at doses above ~ 1 dpa [1,52–54]. The discrepancy at doses above 1 dpa has been attributed to the swelling contributions of large defect aggregates (voids, dislocation loops) which produce macroscopic swelling but do not affect the lattice parameter. The cause of the macroscopic swelling in the alumina specimens irradiated at 200 K in the present study is uncertain since loop formation was not observed and there was not any measurable point defect swelling according to the lattice parameter measurements. One intriguing possibility that needs further investigation is that the step-height expansion may be associated with plastic flow (irradiation creep) that occurs in response to the ion implantation stress [55–57]. A significant amount of conventional radiation creep would not be expected at 200 K in alumina, due to

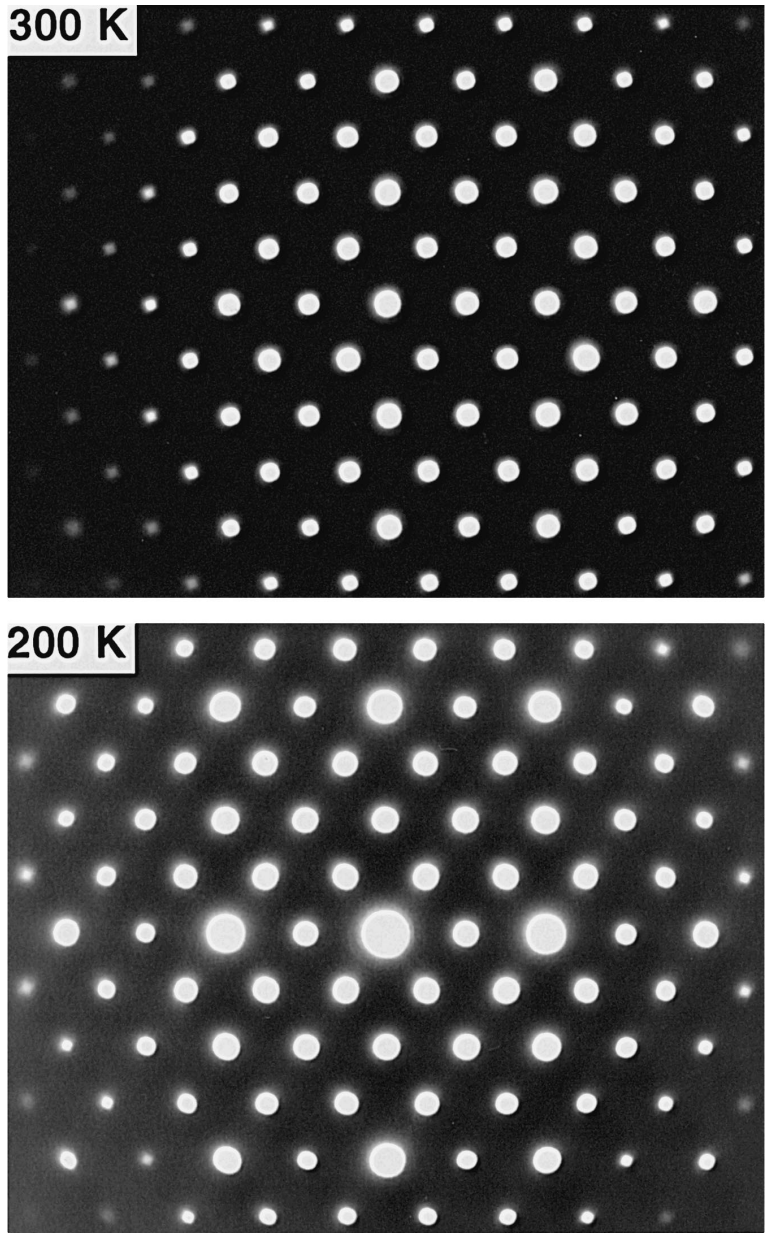

Fig. 8. Comparison of [110] zone axis electron diffraction patterns for spinel irradiated to 5 dpa at 200 and 300 K.

Table 1
Comparison of the step-height and lattice parameter swelling measurements

Specimen	Macroscopic step height swelling, $\Delta V/V$ (%)	Lattice parameter swelling, $\Delta V/V$ (%)
$MgAl_2O_4$ (200 K, 5 dpa)	0.8 ± 0.25	0.9 ± 0.3
$MgAl_2O_4$ (300 K, 5 dpa)	0.9 ± 0.15	0.7 ± 0.2
Al_2O_3 (200 K, 10 dpa)	4.3 ± 0.6	0.1 ± 0.2
Al_2O_3 (300 K, 10 dpa)	3.5 ± 0.4	1.0 ± 0.3

the low point defect mobilities at this temperature. However, it is possible that a non-conventional irradiation creep mechanism such as ionization-enhanced creep may occur in ion-irradiated alumina. Evidence for ionization-induced plastic flow has been reported for ion-irradiated MgO [57].

4. Discussion

Fig. 9 shows the temperature dependence of the step-height swelling for alumina and spinel irradiated with 4

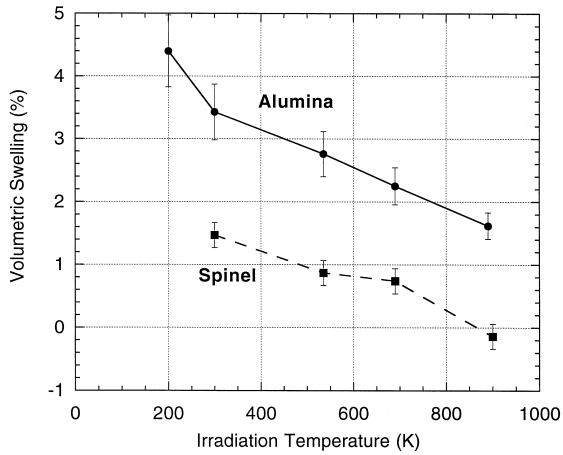

Fig. 9. Volumetric swelling vs. irradiation temperature for alumina and spinel irradiated with 4 MeV Ar^+ ions to a damage level of ~ 10 dpa [38,41,42].

MeV Ar ions to a dose of 10 dpa [38,41,42]. The macroscopic swelling of alumina was significantly higher than that of spinel at all temperatures between 200 and 900 K, in agreement with previous high-dose, high-temperature (670–1100 K) neutron irradiation studies [4,18]. The amount of macroscopic swelling for both alumina and spinel generally decreased with increasing irradiation temperature for a given damage level. This behavior is similar to the well-known results for SiC irradiated to doses of ~ 1 dpa [58–60]. The decrease in swelling with increasing irradiation temperature in ceramics has generally been attributed to the decreased thermal stability of point defect aggregates (dislocation loops and uncollapsed defect clusters) at elevated temperatures. It is interesting to note that the swelling in alumina irradiated at 200 K is higher than expected from extrapolation of the approximately linear temperature dependence at 300–900 K.

The TEM results on Al_2O_3 irradiated to 10 dpa at 300 K imply that the loop unfaulting and network dislocation evolution sequence is initiated at much smaller loop diameters than observed in high temperature irradiations. In previous high temperature (> 770 K) irradiation studies on Al_2O_3, loop unfaulting did not occur until the loop diameter exceeded 15 to 100 nm [2,5], whereas a mixture of faulted and unfaulted loops with a mean diameter of ~ 8 nm was apparently present in the alumina specimen irradiated to 10 dpa at 300 K in the present study. Previous studies on irradiated metals have noted that loop unfaulting is usually triggered by physical impingement of neighboring loops as a result of loop growth, and that the critical size for unfaulting is not well-correlated with stacking fault energy [61,62]. Since the nucleated loop density generally increases with decreasing temperature in irradiated materials, the impingement of growing loops would occur at smaller sizes in specimens irradiated at lower temperatures. Therefore, the apparent unfaulting of dislocation loops in alumina at diameters < 10 nm for an irradiation temperature of 300 K may be attributable to a physical loop interaction effect.

All of the specimens remained crystalline for the investigated irradiation conditions. Transformation from the crystalline to an amorphous state can be initiated by either homogeneous point defect accumulation or heterogeneous displacement cascade collisions [63]. However, a key requirement for amorphization is that the mobility of the radiation defects must be very low, so that thermally-activated recrystallization occurs at a slow rate compared to the defect production [63–65]. The presence of well-defined dislocation loops in spinel irradiated at 200 K (some of which have unfaulted on the cation sublattice and are in the process of rotating on their glide cylinder toward {111} habit planes) implies that significant point defect mobility exists in spinel even at 200 K. Therefore, amorphization would not be expected to occur in spinel irradiated at $\sim 10^{-4}$ dpa/s even after higher doses at 200 K. Conversely, the lack of identifiable dislocation loops in Al_2O_3 at 200 K implies that there is only limited point defect mobility at this temperature, and irradiation to higher dose or at slightly lower temperature (or at a higher damage rate) may induce amorphization in alumina. These conclusions are in agreement with recent irradiation studies which found that spinel is much more difficult to amorphize at cryogenic temperatures (77–200 K) than alumina [27,28,36,47]. The critical temperature above which amorphization of alumina did not occur was found to range from ~ 200 to 250 K for irradiation at dose rates of 0.007 to 0.2 dpa/s, respectively [27].

The 4 MeV Ar ions used for the present irradiation study have an average primary knock-on atom energy of ~ 10 keV, which would produce ~ 100 stable Frenkel pairs in a typical displacement cascade according to the modified Kinchin–Pease displacement model [66]. The loops observed in spinel irradiated at 200 and 300 K had a mean diameter of 4.5 nm, which corresponds to ~ 370 interstitials. Therefore, the formation of these loops appears to be associated with conventional point defect nucleation and growth processes, as opposed to an in-cascade formation process. This conclusion is in accordance with in situ ion irradiation studies by Abe et al. [67], who found that visible loop formation in alumina and spinel occurred after a threshold dose of ~ 0.01 dpa (with subsequent gradual growth of the loops), indicating that loop formation was not associated with direct cascade impact.

The TEM observations performed on alumina in the present study can be used to make a rough estimate of the rate-controlling (slowest) interstitial migration energy. Considering that the formation of visible dislocation loops in Al_2O_3 typically occurs within a dose of ~ 0.01 dpa [67,68], and that the loop density is $N_l = 10^{23}/m^3$ at low irradiation temperatures [68], the interstitial diffusion coefficient (D) can be estimated from the relationship $x =$

$(Dt)^{1/2}$, where $x=(N_1)^{-1/3}=10$ nm and $t=100$ s to achieve a dose of 0.01 dpa for irradiation at 10^{-4} dpa/s. The pre-exponential factor for the diffusion coefficient is given by $D_0 = f_k a_0^2 \nu \exp(\Delta S_m/k) = 1\times10^{-5}$ m^2/s, where f_k is a correlation factor of order unity, a_0^2 is the jump distance (0.275 nm for alumina), $\nu=10^{13}$ s^{-1} is the atomic frequency factor, $\Delta S_m/k=2.5$ is the migration entropy term, and k is Boltzmann's constant [69,70]. Therefore, the estimated upper limit for the rate-controlling interstitial migration enthalpy in Al_2O_3 would be $E_m = kT\ln(D_0/D)=0.77$ eV. This estimate is an upper limit to the migration enthalpy since the loops observed at 300 K might have nucleated within a time less than 100 s (0.01 dpa) and therefore the value of D may be underestimated. Using similar reasoning, the lack of visible loops in the alumina specimen irradiated at 200 K suggests that $E_m >$ 0.52 eV. This estimate is a lower limit to the rate-controlling migration energy since nucleation times longer than 100 s (0.01 dpa) would have led to visible loop formation. An alternative approach to estimate the lower bound of E_m is to assume that the lack of observable loops in Al_2O_3 irradiated at 200 K is due to destruction of the loop nuclei by displacement cascades. Considering that cascade overlap effects would become significant for doses above $\sim$0.1 dpa ($t=1000$ s) and assuming that more than $\sim$100 atoms would need to be collected in order to produce a stable loop nucleus that might survive cascade impact ($x=2$ nm), the estimated lower bound for the rate-controlling interstitial migration energy would be $E_m = 0.61$ eV. Although these estimates for the rate-controlling alumina interstitial migration energy are clearly subject to large uncertainties, the value of $E_m = 0.5$ to 0.8 eV is in agreement with other estimates reported in the literature for Al_2O_3 [16,24,71,72].

5. Conclusions

Alumina generally exhibits significantly higher levels of macroscopic swelling than spinel up to doses of $\sim$10 dpa at all temperatures between 200 and 900 K. The lattice parameter swelling measured for spinel irradiated to 5 dpa at 200 and 300 K is comparable to the macroscopic swelling. The lattice parameter swelling for alumina irradiated to 10 dpa at 200 and 300 K is much smaller than the corresponding macroscopic swelling. Further work is needed to identify the physical process responsible for the macroscopic swelling in alumina irradiated at 200 K, where neither resolvable defect clusters nor lattice parameter swelling was observed. Ionization-induced plastic flow is a possible explanation for the low temperature swelling in alumina.

Amorphization does not occur in spinel or alumina irradiated at 200 and 300 K at a damage rate of $\sim10^{-4}$ dpa/s up to damage levels of 5 and 10 dpa, respectively. The loop microstructure of spinel implies that significant point defect mobility exists at 200 K. Therefore, it is unlikely that spinel would be amorphized even after very high dose irradiations at 200 K for damage rates $<10^{-4}$ dpa/s unless implanted ion effects are important. The lack of observable defect clusters and high macroscopic swelling levels of alumina irradiated at 200 K suggest that amorphization could be induced in this material at higher doses (> 10 dpa) or at a slightly lower temperature, for damage rates of $\sim10^{-4}$ dpa/s. A simplistic analysis suggests that the rate-controlling migration energy for interstitial loop nucleation in alumina is $\sim$0.5 to 0.8 eV.

Acknowledgements

This research was sponsored in part by the Office of Fusion Energy Sciences, US Department of Energy under contract DE-AC05-96OR22464 with Lockheed Martin Energy Research Corp. The authors thank J.W. Jones for preparation of the TEM specimens.

References

[1] R.S. Wilks, J. Nucl. Mater. 26 (1968) 137.
[2] D.G. Howitt, T.E. Mitchell, Philos. Mag. A 44 (1981) 229.
[3] A.Y. Stathopoulos, G.P. Pells, Philos. Mag. A 47 (1983) 381.
[4] F.W. Clinard Jr., G.F. Hurley, L.W. Hobbs, J. Nucl. Mater. 108&109 (1982) 655.
[5] W.E. Lee, M.L. Jenkins, G.P. Pells, Philos. Mag. A 51 (1985) 639.
[6] M.D. Rechtin, Radiat. Eff. 42 (1979) 129.
[7] R.A. Youngman, T.E. Mitchell, F.W. Clinard Jr., G.F. Hurley, J. Mater. Res. 6 (1991) 2178.
[8] G.P. Pells, J. Am. Ceram. Soc. 77 (1994) 368.
[9] S.N. Buckley, S.J. Shaibani, Philos. Mag. Lett. 55 (1987) 15.
[10] S.J. Zinkle, J. Am. Ceram. Soc. 72 (1989) 1343.
[11] S.J. Zinkle, S. Kojima, J. Nucl. Mater. 179–181 (1991) 395.
[12] S.J. Zinkle, in: R.E. Stoller, A.S. Kumar, D.S. Gelles (Eds.), 15th Int. Symp. on Effects of Radiation on Materials, ASTM STP 1125, American Society for Testing and Materials, Philadelphia, 1992, p. 749.
[13] S.J. Zinkle, J. Nucl. Mater. 191–194 (1992) 645.
[14] S.J. Zinkle, Nucl. Instrum. Meth. B 91 (1994) 234.
[15] S.J. Zinkle, J. Nucl. Mater. 219 (1995) 113.
[16] S.J. Zinkle, in: I.M. Robertson et al. (Eds.), Microstructure Evolution During Irradiation, MRS Symp. Proc., vol. 439, Materials Research Society, Pittsburgh, 1997, p. 667.
[17] C. Kinoshita, J. Nucl. Mater. 191–194 (1992) 67.
[18] C. Kinoshita et al., J. Nucl. Mater. 219 (1995) 143.
[19] K. Fukumoto, C. Kinoshita, S. Maeda, K. Nakai, Nucl. Instrum. Meth. B 91 (1994) 252.
[20] Y. Fukushima, T. Yano, T. Maruyama, T. Iseki, J. Nucl. Mater. 175 (1990) 203.
[21] K.E. Sickafus et al., J. Nucl. Mater. 219 (1995) 128.
[22] C. Kinoshita, S.J. Zinkle, J. Nucl. Mater. 233–237 (1996) 100.
[23] L.W. Hobbs, F.W. Clinard Jr., J. Phys. 41 (6) (1980) 232.
[24] S.J. Zinkle, L.L. Snead, submitted to Philos. Mag., presented at Am. Ceram. Soc. 5th Symp. on Fabrication and Properties

of Ceramics for Fusion Energy and Other High Radiation Environments, 1997.
[25] C.W. White et al., Mater. Sci. Rep. 4 (1989) 41.
[26] C.J. McHargue et al., J. Mater. Res. 6 (1991) 2160.
[27] H. Abe, S. Yamamoto, H. Naramoto, Nucl. Instrum. Meth. B 127&128 (1997) 170.
[28] S.X. Wang, L.M. Wang, R.C. Ewing, in: I.M. Robertson et al. (Eds.), Microstructure Evolution During Irradiation, MRS Symp. Proc., vol. 439, Materials Research Society, Pittsburgh, 1997, p. 619.
[29] S.J. Zinkle, L.L. Snead, Nucl. Instrum. Meth. B 116 (1996) 92.
[30] N. Bordes, L.M. Wang, R.C. Ewing, K.E. Sickafus, J. Mater. Res. 10 (1995) 981.
[31] L.M. Wang et al., in: I.M. Robertson et al. (Eds.), Microstructure of Irradiated Materials, MRS Symp. Proc., vol. 373, Materials Research Society, Pittsburgh, 1995, p. 407.
[32] R. Devanathan, N. Yu, K.E. Sickafus, M. Nastasi, Nucl. Instrum. Meth. B 127&128 (1997) 608.
[33] K.E. Sickafus, presented at 8th Int. Conf. on Radiation Effects in Insulators, Catania, Italy, 1995.
[34] N. Yu, K.E. Sickafus, M. Nastasi, Philos. Mag. Lett. 70 (1994) 235.
[35] N. Yu et al., in: R.J. Culbertson et al. (Eds.), Materials Synthesis and Processing using Ion Beams, MRS Symp. Proc., vol. 316, Materials Research Society, Pittsburgh, 1994, p. 69.
[36] K.E. Sickafus, N. Yu, M. Nastasi, Nucl. Instrum. Meth. B 116 (1996) 85.
[37] S. Furuno et al., Nucl. Instrum. Meth. B 127&128 (1997) 181.
[38] G.P. Pells, M.J. Murphy, J. Nucl. Mater. 191–194 (1992) 621.
[39] J.F. Ziegler, J.P. Biersak, U. Littmark, The Stopping and Range of Ions in Solids, Pergamon, New York, 1985.
[40] S.J. Zinkle, C. Kinoshita, J. Nucl. Mater., Proc. Int. Workshop on Defect Production, Accumulation and Materials Performance in Irradiation Environment, Davos, Switzerland, 1997, J. Non-Cryst. Solids 251 (1997) 201.
[41] G.P. Pells, M.J. Murphy, J. Nucl. Mater. 183 (1991) 137.
[42] G.P. Pells, M.J. Murphy, AEA Technology, Harwell Laboratory, Report AEA FUS 148, 1991.
[43] R. Yamada, S.J. Zinkle, G.P. Pells, J. Nucl. Mater. 209 (1994) 191.
[44] S.J. Zinkle, C.P. Haltom, L.C. Jenkins, C.K.H. DuBose, J. Electron. Microsc. Tech. 19 (1991) 452.
[45] W.E. Lee, K.P.D. Lagerlof, J. Electron. Microsc. Tech. 2 (1985) 247.
[46] Y. Satoh, C. Kinoshita, K. Nakai, J. Nucl. Mater. 179–181 (1991) 399.
[47] N. Yu, K.E. Sickafus, M. Nastasi, in: I.M. Robertson et al. (Eds.), Microstructure of Irradiated Materials, MRS Symp. Proc., vol. 373, Materials Research Society, Pittsburgh, 1995, p. 401.
[48] R. Devanathan, K.E. Sickafus, N. Yu, M. Nastasi, Philos. Mag. Lett. 72 (1995) 155.
[49] K.E. Sickafus, N. Yu, R. Devanathan, M. Nastasi, Nucl. Instrum. Meth. B 106 (1995) 573.
[50] Y.G. Chukalkin, V.V. Petrov, V.R. Shtirts, B.N. Goshchitskii, Phys. Status Solidi A 92 (1985) 347.
[51] U. Schmocker, F. Waldner, J. Phys. C 9 (1976) L235.
[52] G.W. Keilholtz, R.E. Moore, Nucl. Appl. 3 (1967) 686.
[53] G.W. Keilholtz, R.E. Moore, H.E. Robertson, Nucl. Tech. 17 (1973) 234.
[54] R.B.J. Roof, W.A. Ranken, J. Nucl. Mater. 55 (1975) 357.
[55] W. Primak, Phys. Rev. B 14 (1976) 4679.
[56] C.A. Volkert, J. Appl. Phys. 70 (1991) 3521.
[57] R. Brenier et al., Nucl. Instrum. Meth. B 80&81 (1993) 1210.
[58] R. Blackstone, E.H. Voice, J. Nucl. Mater. 39 (1971) 319.
[59] R. Price, Nucl. Tech. 35 (1977) 320.
[60] J.E. Palentine, J. Nucl. Mater. 92 (1980) 43.
[61] B.L. Eyre, in: M.T. Robinson, F.W. Young Jr. (Eds.), Fundamental Aspects of Radiation Damage in Metals, vol. II, CONF-751006-P2, National Tech. Inform. Service, Springfield, VA, 1975, p. 729.
[62] S.J. Zinkle, P.J. Maziasz, R.E. Stoller, J. Nucl. Mater. 206 (1993) 266.
[63] H. Trinkaus, Mater. Sci. Forum 248&249 (1997) 3.
[64] W.J. Weber, R.C. Ewing, L.M. Wang, J. Mater. Res. 9 (1994) 688.
[65] A.T. Motta, D.R. Olander, Acta Metall. Mater. 38 (1990) 2175.
[66] M.J. Norgett, M.T. Robinson, I.M. Torrens, Nucl. Eng. Des. 33 (1975) 50.
[67] H. Abe, C. Kinoshita, K. Nakai, J. Nucl. Mater. 179–181 (1991) 917.
[68] S.J. Zinkle, in: I.M. Robertson et al. (Eds.), Microstructure of Irradiated Materials, MRS Symp. Proc., vol. 373, Materials Research Society, Pittsburgh, 1995, p. 287.
[69] W.D. Kingery, H.K. Bowen, D.R. Uhlmann, Introduction to Ceramics, 2nd ed., Wiley, New York, 1976.
[70] K.P.D. Lagerlof, T.E. Mitchell, A.H. Heuer, J. Am. Ceram. Soc. 72 (1989) 2159.
[71] W.D. Kingery, J. Nucl. Mater. 24 (1967) 21.
[72] I.K. Abdukadyrova, Sov. At. Energy 62 (1987) 221.